ELSEVIER

Search for charged Higgs bosons in e^+e^- collisions at $\sqrt{s} = 189$–202 GeV

DELPHI Collaboration

J. Abdallah [v], P. Abreu [t], W. Adam [au], P. Adzic [j], T. Albrecht [o], T. Alderweireld [b],
R. Alemany-Fernandez [h], T. Allmendinger [o], P.P. Allport [u], S. Almehed [w], U. Amaldi [z],
N. Amapane [ap], S. Amato [ar], E. Anashkin [ag], A. Andreazza [y], S. Andringa [t], N. Anjos [t],
P. Antilogus [x], W.-D. Apel [o], Y. Arnoud [l], S. Ask [w], B. Asman [ao], J.E. Augustin [v],
A. Augustinus [h], P. Baillon [h], A. Ballestrero [ap], P. Bambade [r], R. Barbier [x], D. Bardin [n],
G. Barker [o], A. Baroncelli [aj], M. Battaglia [h], M. Baubillier [v], K.-H. Becks [aw],
M. Begalli [f], A. Behrmann [aw], T. Bellunato [h], N. Benekos [ac], A. Benvenuti [e], C. Berat [l],
M. Berggren [v], L. Berntzon [ao], D. Bertrand [b], M. Besancon [ak], N. Besson [ak], D. Bloch [i],
M. Blom [ab], M. Bonesini [z], M. Boonekamp [ak], P.S.L. Booth [u], G. Borisov [h,s], O. Botner [as],
B. Bouquet [r], T.J.V. Bowcock [u], I. Boyko [n], M. Bracko [an], R. Brenner [as], E. Brodet [af],
J. Brodzicka [p], P. Bruckman [p], J.M. Brunet [g], L. Bugge [ad], P. Buschmann [aw], M. Calvi [z],
T. Camporesi [h], V. Canale [ai], F. Carena [h], C. Carimalo [v], N. Castro [t], F. Cavallo [e],
M. Chapkin [am], Ph. Charpentier [h], P. Checchia [ag], R. Chierici [h], P. Chliapnikov [am],
S.U. Chung [h], K. Cieslik [p], P. Collins [h], R. Contri [k], G. Cosme [r], F. Cossutti [aq],
M.J. Costa [at], B. Crawley [a], D. Crennell [ah], J. Cuevas [ae], J. D'Hondt [b], J. Dalmau [ao],
T. da Silva [ar], W. Da Silva [v], G. Della Ricca [aq], A. De Angelis [aq], W. De Boer [o],
C. De Clercq [b], B. De Lotto [aq], N. De Maria [ap], A. De Min [ag], L. de Paula [ar],
L. Di Ciaccio [ai], A. Di Simone [aj], K. Doroba [av], J. Drees [aw], M. Dris [ac], G. Eigen [d],
T. Ekelof [as], M. Ellert [as], M. Elsing [h], M.C. Espirito Santo [h], G. Fanourakis [j],
D. Fassouliotis [j], M. Feindt [o], J. Fernandez [al], A. Ferrer [at], F. Ferro [k], U. Flagmeyer [aw],
H. Foeth [h], E. Fokitis [ac], F. Fulda-Quenzer [r], J. Fuster [at], M. Gandelman [ar], C. Garcia [at],
Ph. Gavillet [h], E. Gazis [ac], D. Gele [i], T. Geralis [j], R. Gokieli [h,av], B. Golob [an],
G. Gomez-Ceballos [al], P. Goncalves [t], E. Graziani [aj], G. Grosdidier [r], K. Grzelak [av],
J. Guy [ah], C. Haag [o], F. Hahn [h], S. Hahn [aw], A. Hallgren [as], K. Hamacher [aw],
K. Hamilton [af], J. Hansen [ad], S. Haug [ad], F. Hauler [o], V. Hedberg [w], M. Hennecke [o],
H. Herr [h], S.-O. Holmgren [ao], P.J. Holt [af], M.A. Houlden [u], K. Hultqvist [ao], J.N. Jackson [u],
P. Jalocha [p], Ch. Jarlskog [w], G. Jarlskog [w], P. Jarry [ak], D. Jeans [af], E.K. Johansson [ao],
P.D. Johansson [ao], P. Jonsson [x], C. Joram [h], L. Jungermann [o], F. Kapusta [v],
S. Katsanevas [x], E. Katsoufis [ac], R. Keranen [o], G. Kernel [an], B.P. Kersevan [h,an],

A. Kiiskinen[m], B.T. King[u], N.J. Kjaer[h], P. Kluit[ab], P. Kokkinias[j], C. Kourkoumelis[c],
O. Kouznetsov[n], Z. Krumstein[n], M. Kucharczyk[p], J. Kurowska[av], B. Laforge[v],
J. Lamsa[a], G. Leder[au], F. Ledroit[l], L. Leinonen[ao], R. Leitner[aa], J. Lemonne[b],
G. Lenzen[aw], V. Lepeltier[r], T. Lesiak[p], W. Liebig[aw], D. Liko[h,au], A. Lipniacka[ao],
J.H. Lopes[ar], J.M. Lopez[ae], D. Loukas[j], P. Lutz[ak], L. Lyons[af], J. MacNaughton[au],
A. Malek[aw], S. Maltezos[ac], F. Mandl[au], J. Marco[al], R. Marco[al], B. Marechal[ar],
M. Margoni[ag], J.-C. Marin[h], C. Mariotti[h], A. Markou[j], C. Martinez-Rivero[al],
J. Masik[aa], N. Mastroyiannopoulos[j], F. Matorras[al], C. Matteuzzi[z], F. Mazzucato[ag],
M. Mazzucato[ag], R. Mc Nulty[u], C. Meroni[y], W.T. Meyer[a], E. Migliore[ap],
W. Mitaroff[au], U. Mjoernmark[w], T. Moa[ao], M. Moch[o], K. Moenig[h,1], R. Monge[k],
J. Montenegro[ab], D. Moraes[ar], S. Moreno[t], P. Morettini[k], U. Mueller[aw], K. Muenich[aw],
M. Mulders[ab], L. Mundim[f], W. Murray[ah], B. Muryn[q], G. Myatt[af], T. Myklebust[ad],
M. Nassiakou[j], F. Navarria[e], K. Nawrocki[av], S. Nemecek[aa], R. Nicolaidou[ak],
P. Niezurawski[av], M. Nikolenko[n,i], A. Nygren[w], A. Oblakowska-Mucha[q],
V. Obraztsov[am], A. Olshevski[n], A. Onofre[t], R. Orava[m], K. Osterberg[h], A. Ouraou[ak],
A. Oyanguren[at], M. Paganoni[z], S. Paiano[e], J.P. Palacios[u], H. Palka[p],
Th.D. Papadopoulou[ac], L. Pape[h], C. Parkes[u], F. Parodi[k], U. Parzefall[u], A. Passeri[aj],
O. Passon[aw], L. Peralta[t], V. Perepelitsa[at], A. Perrotta[e], A. Petrolini[k], J. Piedra[al],
L. Pieri[aj], F. Pierre[ak], M. Pimenta[t], E. Piotto[h], T. Podobnik[an], V. Poireau[ak], M.E. Pol[f],
G. Polok[p], P. Poropat[aq], V. Pozdniakov[n], P. Privitera[ai], N. Pukhaeva[b,n], A. Pullia[z],
J. Rames[aa], L. Ramler[o], A. Read[ad], P. Rebecchi[h], J. Rehn[o], D. Reid[ab], R. Reinhardt[aw],
P. Renton[af], F. Richard[r], J. Ridky[aa], I. Ripp-Baudot[i], D. Rodriguez[al], A. Romero[ap],
P. Ronchese[ag], E. Rosenberg[a], P. Roudeau[r], T. Rovelli[e], V. Ruhlmann-Kleider[ak],
D. Ryabtchikov[am], A. Sadovsky[n], L. Salmi[m], J. Salt[at], A. Savoy-Navarro[v],
C. Schwanda[au], B. Schwering[aw], U. Schwickerath[h], A. Segar[af], R. Sekulin[ah],
M. Siebel[aw], A. Sisakian[n], G. Smadja[x], O. Smirnova[w], A. Sokolov[am], A. Sopczak[s],
R. Sosnowski[av], T. Spassov[h], M. Stanitzki[o], A. Stocchi[r], J. Strauss[au], B. Stugu[d],
M. Szczekowski[av], M. Szeptycka[av], T. Szumlak[q], T. Tabarelli[z], A.C. Taffard[u],
F. Tegenfeldt[as], F. Terranova[z], J. Timmermans[ab], N. Tinti[e], L. Tkatchev[n], M. Tobin[u],
S. Todorovova[h], B. Tome[t], A. Tonazzo[z], P. Tortosa[at], P. Travnicek[aa], D. Treille[h],
G. Tristram[g], M. Trochimczuk[av], C. Troncon[y], M.-L. Turluer[ak], I.A. Tyapkin[n],
P. Tyapkin[n], S. Tzamarias[j], O. Ullaland[h], V. Uvarov[am], G. Valenti[e], P. Van Dam[ab],
J. Van Eldik[h], A. Van Lysebetten[b], N. van Remortel[b], I. Van Vulpen[ab], G. Vegni[y],
F. Veloso[t], W. Venus[ah], F. Verbeure[b], P. Verdier[x], V. Verzi[ai], D. Vilanova[ak], L. Vitale[aq],
V. Vrba[aa], H. Wahlen[aw], A.J. Washbrook[u], C. Weiser[h], D. Wicke[h], J. Wickens[b],
G. Wilkinson[af], M. Winter[i], M. Witek[p], O. Yushchenko[am], A. Zalewska[p],
P. Zalewski[av], D. Zavrtanik[an], N.I. Zimin[n], A. Zintchenko[n], Ph. Zoller[i], M. Zupan[j]

[a] *Department of Physics and Astronomy, Iowa State University, Ames, IA 50011-3160, USA*
[b] *Physics Department, Universiteit Antwerpen, Universiteitsplein 1, B-2610 Antwerpen, Belgium*
and IIHE, ULB-VUB, Pleinlaan 2, B-1050 Brussels, Belgium
and Faculté des Sciences, Univ. de l'Etat Mons, Av. Maistriau 19, B-7000 Mons, Belgium
[c] *Physics Laboratory, University of Athens, Solonos Str. 104, GR-10680 Athens, Greece*
[d] *Department of Physics, University of Bergen, Allégaten 55, NO-5007 Bergen, Norway*
[e] *Dipartimento di Fisica, Università di Bologna and INFN, Via Irnerio 46, IT-40126 Bologna, Italy*
[f] *Centro Brasileiro de Pesquisas Físicas, rua Xavier Sigaud 150, BR-22290 Rio de Janeiro, Brazil*
and Depto. de Física, Pont. Univ. Católica, C.P. 38071 BR-22453 Rio de Janeiro, Brazil
and Inst. de Física, Univ. Estadual do Rio de Janeiro, rua São Francisco Xavier 524, Rio de Janeiro, Brazil
[g] *Collège de France, Lab. de Physique Corpusculaire, IN2P3-CNRS, FR-75231 Paris Cedex 05, France*
[h] *CERN, CH-1211 Geneva 23, Switzerland*
[i] *Institut de Recherches Subatomiques, IN2P3-CNRS/ULP-BP20, FR-67037 Strasbourg Cedex, France*
[j] *Institute of Nuclear Physics, N.C.S.R. Demokritos, P.O. Box 60228, GR-15310 Athens, Greece*
[k] *Dipartimento di Fisica, Università di Genova and INFN, Via Dodecaneso 33, IT-16146 Genova, Italy*
[l] *Institut des Sciences Nucléaires, IN2P3-CNRS, Université de Grenoble 1, FR-38026 Grenoble Cedex, France*
[m] *Helsinki Institute of Physics, HIP, P.O. Box 9, FI-00014 Helsinki, Finland*
[n] *Joint Institute for Nuclear Research, Dubna, Head Post Office, P.O. Box 79, RU-101 000 Moscow, Russian Federation*
[o] *Institut für Experimentelle Kernphysik, Universität Karlsruhe, Postfach 6980, DE-76128 Karlsruhe, Germany*
[p] *Institute of Nuclear Physics, Ul. Kawiory 26a, PL-30055 Krakow, Poland*
[q] *Faculty of Physics and Nuclear Techniques, University of Mining and Metallurgy, PL-30055 Krakow, Poland*
[r] *Université de Paris-Sud, Lab. de l'Accélérateur Linéaire, IN2P3-CNRS, Bât. 200, FR-91405 Orsay Cedex, France*
[s] *School of Physics and Chemistry, University of Landcaster, Lancaster LA1 4YB, UK*
[t] *LIP, IST, FCUL—Av. Elias Garcia, 14-1°, PT-1000 Lisboa Codex, Portugal*
[u] *Department of Physics, University of Liverpool, P.O. Box 147, Liverpool L69 3BX, UK*
[v] *LPNHE, IN2P3-CNRS, Univ. Paris VI et VII, Tour 33 (RdC), 4 place Jussieu, FR-75252 Paris Cedex 05, France*
[w] *Department of Physics, University of Lund, Sölvegatan 14, SE-223 63 Lund, Sweden*
[x] *Université Claude Bernard de Lyon, IPNL, IN2P3-CNRS, FR-69622 Villeurbanne Cedex, France*
[y] *Dipartimento di Fisica, Università di Milano and INFN-MILANO, Via Celoria 16, IT-20133 Milan, Italy*
[z] *Dipartimento di Fisica, Univ. di Milano-Bicocca and INFN-MILANO, Piazza della Scienza 2, IT-20126 Milan, Italy*
[aa] *IPNP of MFF, Charles Univ., Areal MFF, V Holesovickach 2, CZ-180 00, Praha 8, Czech Republic*
[ab] *NIKHEF, Postbus 41882, NL-1009 DB Amsterdam, The Netherlands*
[ac] *National Technical University, Physics Department, Zografou Campus, GR-15773 Athens, Greece*
[ad] *Physics Department, University of Oslo, Blindern, NO-0316 Oslo, Norway*
[ae] *Dpto. Fisica, Univ. Oviedo, Avda. Calvo Sotelo s/n, ES-33007 Oviedo, Spain*
[af] *Department of Physics, University of Oxford, Keble Road, Oxford OX1 3RH, UK*
[ag] *Dipartimento di Fisica, Università di Padova and INFN, Via Marzolo 8, IT-35131 Padua, Italy*
[ah] *Rutherford Appleton Laboratory, Chilton, Didcot OX11 OQX, UK*
[ai] *Dipartimento di Fisica, Università di Roma II and INFN, Tor Vergata, IT-00173 Rome, Italy*
[aj] *Dipartimento di Fisica, Università di Roma III and INFN, Via della Vasca Navale 84, IT-00146 Rome, Italy*
[ak] *DAPNIA/Service de Physique des Particules, CEA-Saclay, FR-91191 Gif-sur-Yvette Cedex, France*
[al] *Instituto de Fisica de Cantabria (CSIC-UC), Avda. los Castros s/n, ES-39006 Santander, Spain*
[am] *Inst. for High Energy Physics, Serpukov P.O. Box 35, Protvino (Moscow Region), Russian Federation*
[an] *J. Stefan Institute, Jamova 39, SI-1000 Ljubljana, Slovenia*
and Laboratory for Astroparticle Physics, Nova Gorica Polytechnic, Kostanjeviska 16a, SI-5000 Nova Gorica, Slovenia
and Department of Physics, University of Ljubljana, SI-1000 Ljubljana, Slovenia
[ao] *Fysikum, Stockholm University, Box 6730, SE-113 85 Stockholm, Sweden*
[ap] *Dipartimento di Fisica Sperimentale, Università di Torino and INFN, Via P. Giuria 1, IT-10125 Turin, Italy*
[aq] *Dipartimento di Fisica, Università di Trieste and INFN, Via A. Valerio 2, IT-34127 Trieste, Italy*
and Istituto di Fisica, Università di Udine, IT-33100 Udine, Italy
[ar] *Univ. Federal do Rio de Janeiro, C.P. 68528 Cidade Univ., Ilha do Fundão BR-21945-970 Rio de Janeiro, Brazil*
[as] *Department of Radiation Sciences, University of Uppsala, P.O. Box 535, SE-751 21 Uppsala, Sweden*
[at] *IFIC, Valencia-CSIC, and D.F.A.M.N., U. de Valencia, Avda. Dr. Moliner 50, ES-46100 Burjassot (Valencia), Spain*
[au] *Institut für Hochenergiephysik, Österr. Akad. d. Wissensch., Nikolsdorfergasse 18, AT-1050 Vienna, Austria*
[av] *Inst. Nuclear Studies and University of Warsaw, Ul. Hoza 69, PL-00681 Warsaw, Poland*
[aw] *Fachbereich Physik, University of Wuppertal, Postfach 100 127, DE-42097 Wuppertal, Germany*

Abstract

A search for pair-produced charged Higgs bosons was performed in the high energy data collected by the DELPHI detector at LEP II at centre-of-mass energies from 189 GeV to 202 GeV. The three different final states, $\tau\nu\tau\nu$, $c\bar{s}\bar{c}s$ and $c\bar{s}\tau\nu$ were considered. New methods were applied to reject wrong hadronic jet pairings and for the tau identification, where a discriminator based on tau polarisation and polar angles was used. No excess of data compared to the expected Standard Model processes was observed and the existence of a charged Higgs boson with mass lower than 71.5 GeV/c^2 is excluded at the 95% confidence level. © 2002 Published by Elsevier Science B.V.

1. Introduction

The existence of a charged Higgs boson doublet is predicted by several extensions of the Standard Model. Pair-production of charged Higgs bosons occurs mainly via s-channel exchange of a photon or a Z^0 boson. In two-doublet models, the couplings are completely specified in terms of the electric charge and the weak mixing angle, θ_W, and therefore the production cross-section depends only on the charged Higgs boson mass. Higgs bosons couple to mass and therefore decay preferentially to heavy particles, but the details are model dependent. We assume that at LEP energies $\tau\nu_\tau$ pair and a cs quark pair channels saturate the charged Higgs boson decays, and analyses of the three possible final states, $\tau\nu\tau\nu$, $c\bar{s}\bar{c}s$ and $c\bar{s}\tau\nu$, have been performed and are described in this Letter. The Higgs decay branching fraction to leptons has been treated as a free parameter in the combination of the results of these three analyses.

A search for pair-produced charged Higgs bosons was performed in the data collected by DELPHI during the LEP runs at centre-of-mass energies from 189 GeV to 202 GeV. The results reported here update those obtained in an earlier analysis of the DELPHI data limited to the 183 GeV run [1]. Similar searches have been performed by the other LEP experiments [2].

A new technique was developed to improve the discrimination against the hadronic W decays in the search for $H^\pm$ candidates. Improved methods using

the τ polarisation and boson production angles in the leptonic and semileptonic channels were used for rejection of W^+W^- background.

2. Data analysis

Data collected during the years 1998 and 1999 at centre-of-mass energies from 189 GeV to 202 GeV were used. The total integrated luminosity of these data samples is approximately 380 pb^{-1}. The DELPHI detector and its performance have already been described in detail elsewhere [3,4]. [2]

Signal samples were simulated using the HZHA generator [5]. The background estimates from the different Standard Model processes were based on the following event generators: PYTHIA [6] for $q\bar{q}(\gamma)$, KORALZ [7] for $\mu^+\mu^-$ and $\tau^+\tau^-$, BABAMC [8] for e^+e^- and EXCALIBUR [9] for four-fermion final states. Two-photon interactions were generated with TWOGAM [10] for hadronic final states, BDK [11] for electron final states and BDKRC [11] for other leptonic final states.

In all three analyses the final background rejection was performed by using a likelihood technique. For each of the N discriminating variables, the fractions $F_i^{\mathrm{HH}}(x_i)$ and $F_i^{\mathrm{bkg}}(x_i)$ of, respectively, H$^+$H$^-$ and background events, corresponding to a given value x_i of the ith variable, were extracted from samples of simulated H$^+$H$^-$ and background events

---

[2] The coordinate system used has the z-axis parallel to the electron beam, and the polar angle calculated with respect to this axis.

Table 1
The total number of events observed and expected backgrounds in the leptonic channel after the different cuts used in the analysis. The last column shows the efficiency for a charged Higgs boson signal with $m_{H^\pm} = 75$ GeV/c^2

Cut	Data	Total bkg.	4-Fermion	Other bkg.	ε_{75}
Leptonic selection	106274	108275	591	107684	73.6%
Acoplanarity cut	10841	10519	452	10068	60.0%
Energy/momentum cuts	360	359	343	16	45.6%
τ identification	39	39.7	36.3	3.4	34.0%

normalised to equal size. The signal likelihood was computed as the normalised product of these individual fractions, $\prod_{i=1,N} F_i^{HH}(x_i)/(\prod_{i=1,N} F_i^{HH}(x_i) + \prod_{i=1,N} F_i^{bkg}(x_i))$.

2.1. The leptonic channel

The signature for $H^+H^- \to \tau^+\nu_\tau\tau^-\bar{\nu}_\tau$ is large missing energy and momentum and two acollinear and acoplanar [3] jets containing either a lepton or one or a few hadrons. Tight requirements for efficient operation of the most important sub-detectors were used in this analysis in order to ensure good quality of the tracks. These result in slightly smaller integrated luminosities than in the hadronic channel (see Table 4).

2.1.1. Event preselection

To select leptonic events a total charged particle multiplicity between 2 and 6 was required. All particles in the event were clustered into jets using the LUCLUS algorithm [6] ($d_{join} = 6.5$ GeV/c) and only events with two reconstructed jets were retained. Both jets had to contain at least one charged particle and at least one jet had to contain not more than one charged particle. The angle between the two jets was required to be larger than 30°.

Two-fermion and two-photon events were rejected by requiring an acoplanarity larger than 13° if both jets were in the barrel region (43° < θ < 137°) and larger than 25° otherwise.

---

[3] The acoplanarity is defined as the complement of the angle between the two jets projected onto the plane perpendicular to the beam.

The two-photon background was further reduced by the following energy and momentum requirements: the sum of the jet energies multiplied by the sines of their jet angles to the beam direction, $E_\perp$, was required to be larger than $0.08\sqrt{s}$ if both jets were in the barrel region and larger than $0.1\sqrt{s}$ in other cases; the total transverse momentum, $p_\perp$, to be greater than $0.04\sqrt{s}$; the total energy detected within 30° around the beam axis to be less than $0.1\sqrt{s}$; and the total energy outside this region to be greater than $0.1\sqrt{s}$.

Additional τ identification cuts were applied to reject WW events where the W's have not decayed to $\tau\nu$. If the τ jet was identified as an electron it had to have a momentum below $0.13\sqrt{s}$ and an electromagnetic energy below $0.14\sqrt{s}$. For muons the momentum had to be below $0.13\sqrt{s}$. If a τ decay candidate particle was not identified as either a muon or an electron, it was considered to be a hadron and accepted as a τ decay particle without further requirements. Events in which the invariant mass of either of the jets was more than 3 GeV/c^2 were rejected.

The effects of the $\tau^+\nu_\tau\tau^-\bar{\nu}_\tau$ selection cuts are shown in Table 1 for the combined 189–202 GeV sample.

2.1.2. Final background discrimination

After these selections most of the remaining background consists of $W^+W^- \to \tau^+\nu_\tau\tau^-\bar{\nu}_\tau$ events. Events from both the H^+H^- signal and the W^+W^- background have similar topologies and due to the presence of missing neutrinos in the decay of each of the bosons, it is not possible to reconstruct the boson mass. There are two important differences, however, that were used in order to discriminate the signal from
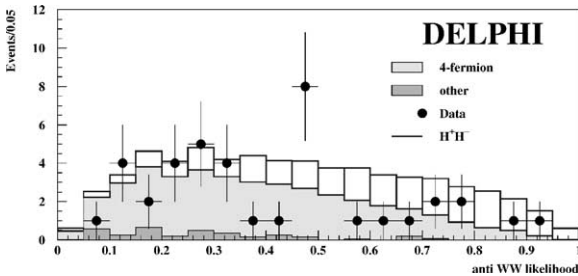
Fig. 1. Distribution of the anti-WW likelihood for leptonic events at 189–202 GeV. The expected histogram for a 75 GeV/c^2 charged Higgs boson signal has been normalised to the production cross-section and 100% leptonic branching ratio and added to the backgrounds.

the W^+W^- background: the boson polar angle and the τ polarisation.

Assuming that the ν_τ has a definite helicity, the polarisation (P_τ) of tau leptons originating from heavy boson decays is determined entirely by the properties of weak interactions and the nature of the parent boson. The helicity configuration for the signal is $H^- \to \tau_R^- \bar{\nu}_{\tau R}$ ($H^+ \to \tau_L^+ \nu_{\tau L}$) and for the $W^\pm$ boson background it is $W^- \to \tau_L^- \bar{\nu}_{\tau R}$ ($W^+ \to \tau_R^+ \nu_{\tau L}$) resulting in $P_\tau^H = +1$ and $P_\tau^W = -1$. The angular and momentum distributions depend on polarisation and it is possible to build estimators of the τ polarisation to discriminate between the two contributions.

The τ decays were classified into the following categories: e, μ, π, $\pi + n\gamma$, 3π and others. The information on the τ polarisation was extracted from the observed kinematic distributions of the τ decay products, i.e., their angles and momenta. These estimators are equivalent to those used at LEP I [12]. For charged Higgs boson masses close to the threshold, the boost of the bosons is relatively small and the τ energies are similar to those of the τ's from Z^0 decays (40–50 GeV).

A likelihood to separate the signal from the W^+W^- background was built using four variables: the estimators of the τ polarisation and the polar angle of the decay products of both τ's. The distribution of that likelihood for data, expected backgrounds and a 75 GeV/c^2 charged Higgs boson is shown in Fig. 1.

2.2. The hadronic channel

In the fully hadronic decay channel, each charged Higgs boson is expected to decay into a $c\bar{s}$ pair, producing a four-jet final state. The two sources of background in this channel are the $q\bar{q}gg$ QCD background and fully hadronic four-fermion final states. In the four-fermion state background the significance of the Z^0Z^0 pairs in the analysis is very small compared to the W^+W^- pairs. This is due to the lower cross-section for Z^0Z^0 pair production and because the reconstructed Z^0Z^0 pair masses are concentrated at high masses, around the Z^0 boson mass, out of the sensitivity reach of the analysis. Therefore, the four-fermion sample is referred to as W^+W^- in the rest of the Letter.

2.2.1. Event preselection

Events were clustered into four jets using the Durham algorithm [13]. The particle quality requirements and the first level hadronic four-jet event selection followed in this analysis were the same as for the DELPHI neutral Higgs analysis [14].

In order to reject three-jet like QCD background events more effectively, the Durham clustering parameter value for transition from four to three jets ($y_{4\to3}$) was required to be greater than 0.003. Events with a clear topology of more than four jets were rejected by requiring the $y_{5\to4}$ value for transition from five to four jets to be below 0.010 because of their worse di-jet mass resolution after forcing them into four jets.

Energy–momentum conservation was imposed by performing a 4-C fit on these events and the difference between the two di-jet masses for each jet pairing was computed. A 5-C fit, assuming equal boson masses, was applied in order to improve the di-jet mass resolution. The di-jet combination giving the smallest 5-C fit χ^2 was selected for the mass reconstruction. Events for which the 5-C fit χ^2 divided by the number of degrees of freedom exceeded 1.5 or the difference of the masses computed with the same pairing after the 4-C fit exceeded 15 GeV/c^2 were rejected.

2.2.2. Final background rejection

The largest contribution to the part of the selected sample of W^+W^- events whose reconstructed mass is below the W mass peak comes from picking one

Table 2
The total number of events observed and expected backgrounds in the hadronic channel after the different cuts used in the analysis. The last column shows the efficiency for a charged Higgs boson signal with $m_{H^\pm} = 75$ GeV/c^2

Cut	Data	Total bkg.	4-Fermion	Other bkg.	ε_{75}
4-jet presel.	4156	3981.8	2515.0	1466.8	84.0%
Durham y_{cut}	3066	2945.0	2110.0	835.0	71.4%
χ^2	2397	2340.0	1760.5	579.5	60.5%
Mass diff.	1755	1708.6	1365.0	343.6	50.0%
Anti-QCD	857	844.5	767.0	77.5	36.5%
Anti-WW	653	645.7	577.8	67.9	33.2%

of the wrong di-jet pairings. These wrongly paired events are characterised by a larger difference between the masses of the two di-jets, i.e., the two boson candidates. As the initial quark–antiquark pairs are connected by a QCD colour field, in which the hadrons are produced in the fragmentation process, the wrongly paired events can also be identified using a method of colour connection reconstruction [15].

The colour connection reconstruction method is based on the fact that, in the rest frame of the correctly paired initial quark–antiquark pair, the hadrons that are produced in this colour string should have small transverse momenta relative to the quark–antiquark pair axis. This could be distorted by hard gluon emission but such events are suppressed with the $y_{5\to4}$ Durham parameter cut. When boosted into a rest frame of a wrongly paired quark pair the transverse momenta of the particles relative to the quark–quark axis are larger. The correct pairing is found by calculating the sum of transverse particle momenta in each of the three possible pairing hypotheses. The pairing chosen using the colour connection reconstruction is compared to the pairing chosen using the minimisation of the χ^2 of the 5-C kinematical fit. The output of this comparison, called $p_\perp$-veto, is either agreement or disagreement and it is used later in the analysis as one of the variables in the background rejection likelihood.

The production polar angle of the positively charged boson discriminates between W^+W^- and Higgs pairs. This angle is reconstructed as the polar angle of the di-jet with the higher sum of jet charges, where the jet charge is calculated as a momentum weighted sum of the charges of the particles in the jet [16]. The distribution of this variable allows the discrimination of the signal from the background of wrongly paired

W^+W^- events and QCD events, even though in these latter cases the variable does not correspond to a true boson production angle.

Since the charged Higgs boson is expected to decay to $c\bar{s}$ in its hadronic decay mode, the QCD and W^+W^- backgrounds can be partially suppressed by selecting final states consistent with being $c\bar{s}\bar{c}s$. A flavour tagging algorithm has been developed for the study of multiparton final states. [4] This tagging is based on nine discriminating variables: three of them are related to the identified lepton and hadron content of the jet, two depend on kinematical variables and four on the reconstructed secondary decay structure. The finite lifetime of c (charm) particles is exploited to distinguish between c and light quark jets, while the c mass and decay multiplicity are used to discriminate against b jets. Furthermore, s and c jets can be distinguished from u and d jets by the presence of an identified energetic kaon. Charged hadrons have been identified using the combined response of RICH and TPC dE/dx [18]. The responses of the flavour tagging algorithm for the individual jets are further combined into an event $c\bar{s}\bar{c}s$ probability.

The four variables described above: di-jet pair mass difference, the $p_\perp$-veto, di-jet momentum polar angle and event $c\bar{s}\bar{c}s$ probability, were combined to form an event anti-WW likelihood function separating W^+W^- events from H^+H^- events. The response of this likelihood also discriminates H^+H^- from the QCD background events.

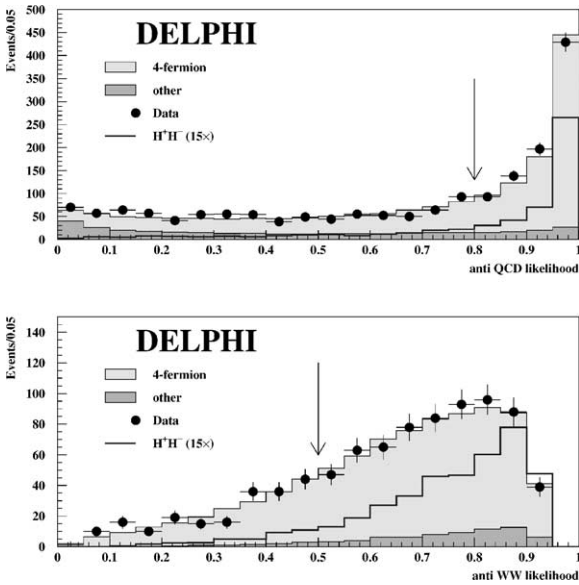[4] A similar jet flavour tagging technique has been used in a determination of $|V_{cs}|$ at LEP II [17].

Fig. 2. Distributions of the anti-QCD and anti-WW likelihoods for hadronic events at 189–202 GeV. The anti-QCD likelihood is plotted on the preselection level and the anti-WW likelihood after a cut on the anti-QCD likelihood. The generated H^+H^- signal mass is 75 GeV/c^2 and the signal histograms have been normalised to the production cross-section and 100% hadronic branching ratio, multiplied by a factor of 15 and superimposed on the background histograms. The arrows indicate the cut values, below which events were rejected.

An anti-QCD likelihood was formed using all four variables which were used in the anti-WW likelihood and, in addition, two variables which can be used to separate QCD background from pair-produced bosons: the clustering algorithm parameter $y_{4\to3}$ and the event acoplanarity.

The effects of the different sets of cuts are shown in Table 2 for the combined 189–202 GeV sample. The distribution of the anti-QCD likelihood on the preselection level and the distribution of the anti-WW likelihood after a cut on the anti-QCD likelihood are shown in Fig. 2. The reconstructed mass distribution for data, expected backgrounds and signal after the anti-QCD and anti-WW cuts is shown in Fig. 3.

2.3. The semileptonic channel

In this channel one of the charged Higgs bosons decays into a $c\bar{s}$ quark pair, while the other decays into $\tau\nu_\tau$. Such an event is characterised by two hadronic
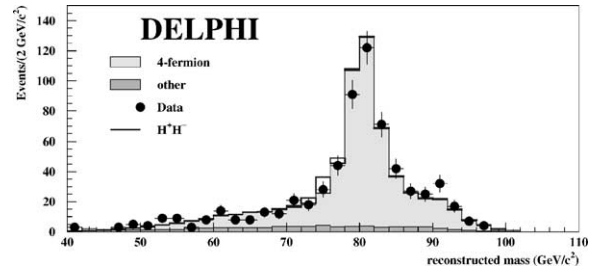

Fig. 3. Reconstructed mass distribution of hadronic events at 189–202 GeV at the final selection level. The generated H^+H^- signal mass is 75 GeV/c^2 and the signal histogram has been normalised to the production cross-section and 100% hadronic branching ratio and added to the backgrounds.

jets, a τ candidate and missing energy carried by the neutrinos. The dominating background processes are QCD $q\bar{q}g$ event production and semileptonic decays of W^+W^-. The same requirements for efficient operation of the most important sub-detectors were used as in the analysis of the leptonic channel.

2.3.1. Event preselection and τ selection

At least 15 particles, of which at least 8 were charged, were required. The total energy of the observed particles had to exceed $0.30\sqrt{s}$. The missing transverse momentum had to be greater than $0.08\sqrt{s}$ and the modulus of the cosine of the angle between the missing momentum and the beam had to be less than 0.8. Events were also required to have no neutral particles with energy above 40 GeV.

After clustering into three jets using the Durham algorithm, the clustering parameter $y_{3\to2}$ was required to be greater than 0.003, and each jet had to contain at least one charged particle. The jet with the smallest charged particle multiplicity was treated as the τ candidate and if two or more of the jets had the same number of charged particles, the jet with smallest energy was chosen. The τ candidate was required to have no more than six particles, of which no more than three were charged.

2.3.2. Final background rejection

The mass of the decaying bosons was reconstructed using a constrained fit requiring energy and momentum conservation with the known beam energy and imposing the masses of the two bosons to be equal. The three components of the momentum vector of the ν_τ
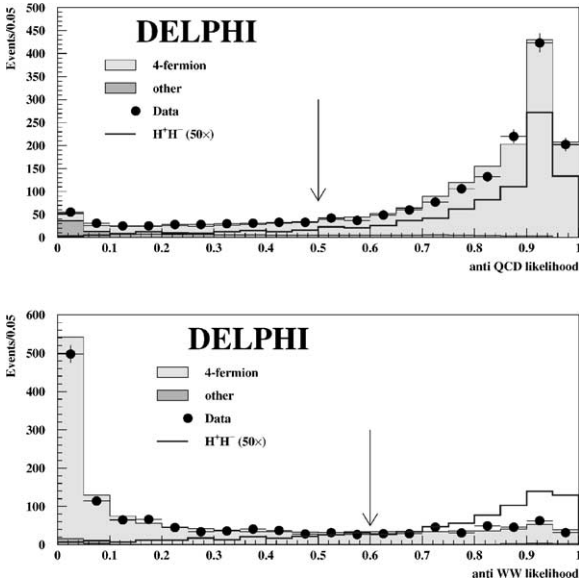
Fig. 4. Distributions of the anti-QCD and anti-WW likelihoods for semileptonic events at 189–202 GeV. The anti-QCD likelihood is plotted on the τ selection level and the anti-WW likelihood after a cut on the anti-QCD likelihood. The generated H^+H^- signal mass is 75 GeV/c^2 and the signal histograms have been normalised to the production cross-section and 50% leptonic branching ratio, multiplied by a factor of 50 and superimposed on the background histograms. The arrows indicate the cut values, below which events were rejected.
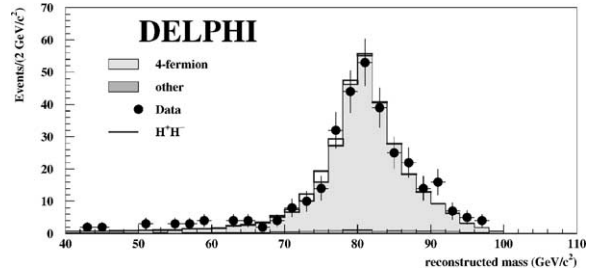

Fig. 5. Reconstructed mass distribution of semileptonic events at 189–202 GeV at the final selection level. The generated H^+H^- signal mass is 75 GeV/c^2 and the signal histogram has been normalised to the production cross-section and 50% leptonic branching ratio and added to the backgrounds.

Table 3
The total number of events observed and expected backgrounds in the semi-leptonic channel after the different cuts used in the analysis. The last column shows the efficiency for a charged Higgs boson signal with $m_{H^\pm} = 75$ GeV/c^2

Cut	Data	Total bkg.	4-Fermion	Other bkg.	ε_{75}
Preselection	6395	6104.8	3043.8	3061.0	81.6%
τ selection	2149	2144.0	1788.0	356.0	58.1%
χ^2	1667	1699.0	1552.4	146.6	50.4%
Likelihoods	325	307.4	292.4	15.0	33.8%

and the magnitude of the τ momentum were treated as free parameters, reducing the number of degrees of freedom of the fit from 5 to 1. Only events with a reconstructed mass above 40 GeV/c^2 and a χ^2 below 2 were selected.

Separate likelihood functions were defined to distinguish the signal events from the QCD and the W^+W^- backgrounds, in a manner similar to that used for the other channels described above.

To define the anti-QCD likelihood, the acollinearity of the event (after forcing the event into two jets), the polar angle of the missing momentum, the logarithm of the clustering parameter $y_{3\to2}$, and the product of the τ jet energy and the smaller of the two angles between the τ jet and one of the other jets were used as discriminating variables.

For the event anti-WW likelihood the variables used were the reconstructed polar angle of the negatively charged boson (where the charge was determined from the leading charged particle of the τ jet), the angle

between the boson and the τ in the boson rest frame, the energy of the τ jet, the classification of the decay of the τ candidate (e, μ, π, $\pi + n\gamma$, 3π and others), and the cs probability of the hadronic di-jet.

The effects of the different sets of cuts are shown in Table 3 for the combined 189–202 GeV sample. The distribution of the anti-QCD likelihood on the τ selection level and the distribution of the anti-WW likelihood after a cut on the anti-QCD likelihood are shown in Fig. 4. The reconstructed mass distribution for data, expected backgrounds and signal after anti-QCD and anti-WW cuts is shown in Fig. 5.

3. Results

3.1. Selection efficiencies and uncertainties

The number of real data and background events and the estimated efficiencies for these selections for two different $H^\pm$ masses are summarised in Table 4 for

the three final states. The quoted errors include the systematic uncertainties in the expected background and the signal efficiency. Small contributions to these uncertainties are due to uncertainties in the luminosity measurement and in the cross-section estimates of the generated Monte Carlo samples.

The event selection and systematic errors in the leptonic analysis are very similar to those in the DELPHI leptonic W^+W^- analysis [19]. The largest part of the background and signal efficiency uncertainties in the leptonic channel is due to the limited simulation statistics available. Combining these uncertainties gives a total uncertainty of the order of 10% in the background rate and 5% in the signal efficiency.

The largest contribution in the hadronic and semileptonic analyses is due to differences in the distributions of the preselection and likelihood variables in data and simulation. The systematic error on the efficiency of the common DELPHI hadronic four-jet preselection has been estimated to be ±4% [14]. The uncertainties related to the other selection variables have

been estimated by comparing the shapes of the variable distributions in data and simulation. This has been done at the preselection level where the background event rate is so large that a possible signal would have no effect on the global shapes of the variables. The agreement of all variables has been found to be satisfactory to the level of a few percent. Combining these errors, a total uncertainty of 6% has been estimated for the background rate and signal efficiency in the hadronic channel. In the semileptonic channel the combined background error estimate is 6 to 9% depending on the energy sample and the error of the signal efficiency is of the order of 6%. The combined error estimates are included in Table 4.

3.2. Determination of the mass limit

No significant signal-like excess of events was observed in any of the three final states investigated. We find an agreement between data and background expectations also in the mass region around 68 GeV/c^2

Table 4

Integrated luminosity, observed number of events, expected number of background events and signal efficiency (70 GeV/c^2 and 75 GeV/c^2 masses) for different decay channels and centre-of-mass energies

Channel	$\sqrt{s}$	Luminosity	Data	Total bkg.	ε_{70}	ε_{75}
$\tau\nu\tau\nu$	189	153.8	16	15.0±1.5	32.3±1.6%	34.2±1.6%
$\tau\nu\tau\nu$	192	24.5	3	2.8±0.3	33.6±1.6%	34.2±1.6%
$\tau\nu\tau\nu$	196	72.4	10	8.6±0.8	33.6±1.6%	34.2±1.6%
$\tau\nu\tau\nu$	200	81.8	8	9.0±0.9	33.6±1.6%	33.5±1.6%
$\tau\nu\tau\nu$	202	39.4	2	4.4±0.4	33.6±1.6%	33.5±1.6%
$cscs$	189	154.3	288	267.8±16.1	36.2±2.0%	33.1±2.0%
$cscs$	192	25.5	36	42.7±2.6	36.2±2.0%	33.1±2.0%
$cscs$	196	77.1	141	130.0±7.8	34.5±2.0%	33.8±2.0%
$cscs$	200	83.9	133	138.8±8.3	33.9±2.0%	33.5±2.0%
$cscs$	202	40.6	55	66.2±4.1	33.9±2.0%	33.5±2.0%
$cs\tau\nu$	189	153.8	126	118.8±6.9	33.0±1.8%	31.8±1.7%
$cs\tau\nu$	192	24.5	29	21.2±1.9	36.6±2.2%	35.2±2.1%
$cs\tau\nu$	196	72.4	76	62.2±5.5	36.6±2.2%	35.2±2.1%
$cs\tau\nu$	200	81.8	67	71.1±6.4	35.2±2.1%	35.3±2.1%
$cs\tau\nu$	202	39.4	27	34.1±3.1	35.2±2.1%	35.3±2.1%

where the L3 Collaboration has reported an excess using data collected at the same centre-of-mass energies [2]. A lower limit for a charged Higgs boson mass was derived at 95% confidence level as a function of the leptonic Higgs decay branching ratio $BR(H \to \tau \nu_\tau)$. The confidence in the signal hypothesis, CL_s, was calculated using a likelihood ratio technique [20].

The background and signal probability density functions of one or two discriminating variables in each channel were used. The data samples collected at the five different centre-of-mass energies were treated separately in the combination. Correlations between the systematic uncertainties in different centre-of-mass energies were not included. In the hadronic and semileptonic channels the two discriminating variables were the reconstructed mass and the anti-WW likelihood; in the leptonic channel only one background discrimination likelihood was used since mass reconstruction is not possible. The distributions of the discriminating variable for signal events, obtained by the simulation at different $H^\pm$ mass values for each $\sqrt{s}$, were interpolated for intermediate mass values. To obtain the expected signal rate at any given mass the signal efficiencies were fitted with polynomial functions.

A Gaussian smearing of the central values of the number of expected background events by their estimated uncertainties was introduced in the limit derivation program.

The results are summarised in Fig. 6. A lower $H^\pm$ mass limit of $M_{\mathrm{H}}^\pm > 71.5$ GeV/c^2 can be set at the 95% confidence level, independently of the branching ratio $BR(H \to \tau \nu_\tau)$. The production cross-section for the charged Higgs bosons signal at this mass (71.5 GeV/c^2) and a centre-of-mass energy of 202 GeV would be 0.255 pb. The median of the limits obtained from a large number of simulated experiments is 73.3 GeV/c^2.

4. Conclusion

A search for pair-produced charged Higgs bosons was performed using the full statistics collected by DELPHI at LEP at centre-of-mass energies from 189 GeV to 202 GeV analysing the $\tau \nu \tau \nu$, $c\bar{s}\bar{c}s$ and $c\bar{s}\tau\nu$ final states. No significant excess of candidates
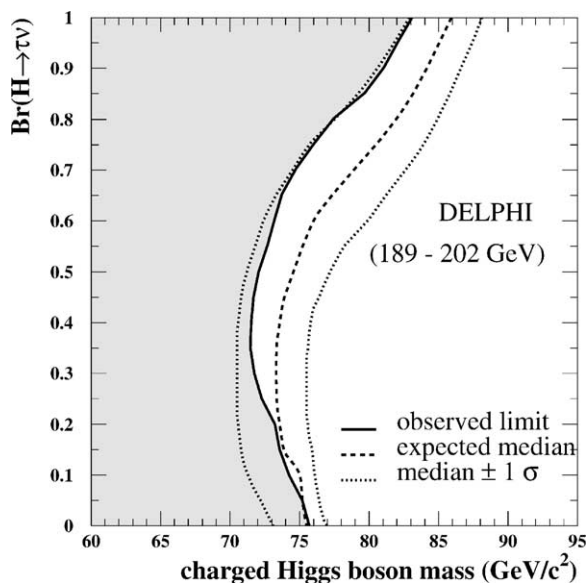

Fig. 6. The 95% confidence level observed and expected exclusion regions for $H^\pm$ in the plane $BR(H \to \tau \nu_\tau)$ vs. $M_{\mathrm{H}}^\pm$ obtained from a combination of the search results in the fully leptonic, hadronic and semileptonic decay channels at $\sqrt{s} = 189$–202 GeV. The expected median of the lower mass limits has been obtained from a large number of simulated experiments. The median is the value which has 50% of the limits of the simulated experiments below it and the $\pm 1\sigma$ lines correspond similarly to 84% and 16% of the simulated experiments.

was observed and a lower limit on the charged Higgs mass of 71.5 GeV/c^2 is set at 95% confidence level. The sensitivity of the DELPHI charged Higgs boson search is comparable to the ones of the other LEP Collaborations [21].

Acknowledgements

References

[1] P. Abreu et al., DELPHI Collaboration, Phys. Lett. B 460 (1999) 484.

[2] R. Barate et al., ALEPH Collaboration, Phys. Lett. B 487 (2000) 253;
M. Acciarri et al., L3 Collaboration, Phys. Lett. B 496 (2000) 34;
G. Abbiendi et al., OPAL Collaboration, Eur. Phys. J. C 7 (1999) 407.

[3] P. Aarnio et al., DELPHI Collaboration, Nucl. Instrum. Methods A 303 (1991) 233.

[4] P. Abreu et al., DELPHI Collaboration, Nucl. Instrum. Methods A 378 (1996) 57.

[5] P. Janot, in: CERN Report 96-01, Vol. 2, p. 309.

[6] T. Sjöstrand, Comput. Phys. Commun. 82 (1994) 74.

[7] S. Jadach, B.F.L. Ward, Z. Was, Comput. Phys. Commun. 79 (1994) 503.

[8] F.A. Berends, R. Kleiss, W. Hollik, Nucl. Phys. B 304 (1988) 712.

[9] F.A. Berends, R. Pittau, R. Kleiss, Comput. Phys. Commun. 85 (1995) 437.

[10] S. Nova, A. Olchevski, T. Todorov, in: CERN Report 96-01, Vol. 2. p. 224;
T. Alderweireld et al., in: CERN Report 2000-009, p. 219.

[11] F.A. Berends, P.H. Daverveldt, R. Kleiss, Comput. Phys. Commun. 40 (1986) 271, 285 and 309.

[12] P. Abreu et al., DELPHI Collaboration, Z. Phys. C 67 (1995) 183.

[13] S. Catani et al., Phys. Lett. B 269 (1991) 432.

[14] P. Abreu et al., DELPHI Collaboration, Eur. Phys. J. C 10 (1999) 563.

[15] E. Norrbin, T. Sjöstrand, Phys. Rev. D 55 (1997) 55.

[16] P. Abreu et al., DELPHI Collaboration, Phys. Lett. B 502 (2001) 9.

[17] P. Abreu et al., DELPHI Collaboration, Phys. Lett. B 439 (1998) 209.

[18] M. Battaglia, P.M. Kluit, Nucl. Instrum. Methods A 433 (1999) 252.

[19] P. Abreu et al., DELPHI Collaboration, Phys. Lett. B 479 (2000) 89.

[20] A.L. Read, in: CERN Report 2000-005, p. 81.

[21] ALEPH, DELPHI, L3 and OPAL Collaborations, Searches for Higgs bosons: preliminary combined results using LEP data collected at energies up to 202 GeV, CERN-EP 2000-055.